The FEBS Journal

FEBS PRESS science publishing by scientists

A pathway for assembling $[4Fe\text{-}4S]^{2+}$ clusters in mitochondrial iron–sulfur protein biogenesis

Veronica Nasta[1,2], Dafne Suraci[1], Spyridon Gourdoupis[1], Simone Ciofi-Baffoni[1,2] and Lucia Banci[1,2]

1 Magnetic Resonance Center CERM, University of Florence, Italy
2 Department of Chemistry, University of Florence, Italy

Keywords
BOLA3; GLRX5; iron–sulfur protein; mitochondrial iron–sulfur cluster assembly machinery; NFU1

Correspondence
L. Banci, Magnetic Resonance Center CERM, University of Florence, Via Luigi Sacconi 6, 50019 Sesto Fiorentino, Florence, Italy
Tel: +39-055-4574273
E-mail: banci@cerm.unifi.it
S. Ciofi-Baffoni, Magnetic Resonance Center CERM, University of Florence, Via Luigi Sacconi 6, 50019 Sesto Fiorentino, Florence, Italy
Tel: +39-055-4574192
E-mail: ciofi@cerm.unifi.it

Veronica Nasta, Dafne Suraci, Spyridon Gourdoupis contributed equally to this work

(Received 5 August 2019, revised 8 October 2019, accepted 13 November 2019)

doi:10.1111/febs.15140

During its late steps, the mitochondrial iron–sulfur cluster (ISC) assembly machinery leads to the formation of [4Fe-4S] clusters. *In vivo* studies revealed that several proteins are implicated in the biosynthesis and trafficking of [4Fe-4S] clusters in mitochondria. However, they do not provide a clear picture into how these proteins cooperate. Here, we showed that three late-acting components of the mitochondrial ISC assembly machinery (GLRX5, BOLA3, and NFU1) are part of a ISC assembly pathway leading to the synthesis of a $[4Fe\text{-}4S]^{2+}$ cluster on NFU1. We showed that the $[2Fe\text{-}2S]^{2+}$ GLRX5-BOLA3 complex transfers its cluster to monomeric apo NFU1 to form, in the presence of a reductant, a $[4Fe\text{-}4S]^{2+}$ cluster bound to dimeric NFU1. The cluster formation on NFU1 does not occur with $[2Fe\text{-}2S]^{2+}$ GLRX5, and thus, the [4Fe-4S] cluster assembly pathway is activated only in the presence of BOLA3. These results define NFU1 as an 'assembler' of [4Fe-4S] clusters, that is, a protein able of converting two $[2Fe\text{-}2S]^{2+}$ clusters into a $[4Fe\text{-}4S]^{2+}$ cluster. Finally, we found that the $[4Fe\text{-}4S]^{2+}$ cluster bound to NFU1 has a coordination site which is easily accessible to sulfur-containing ligands, as is typically observed in metallochaperones. This finding supports a role for NFU1 in promoting rapid and controlled cluster-exchange reaction.

Introduction

Mitochondria play a key role in the maturation of iron–sulfur (Fe-S) proteins [1,2]. Within mitochondria, the biosynthesis of Fe-S clusters and their insertion into mitochondrial apo target proteins is assisted by at least 17 proteins forming the mitochondrial iron–sulfur cluster (ISC) assembly machinery [2]. In this machinery, [4Fe-4S] clusters are formed by a specific system, including ISCA1 and ISCA2 proteins, that generate a [4Fe-4S] cluster by coupling two [2Fe-2S] clusters [1,2]. The [4Fe-4S] clusters are then transferred to apo target proteins with the assistance of the so-called ISC targeting factors. One of these factors is the

Abbreviations
BMRB, biological magnetic resonance bank; Fe-S, iron–sulfur; GSH, reduced glutathione; HADDOCK, high ambiguity-driven protein–protein docking; HSQC, heteronuclear single quantum coherence; IPTG, isopropyl β-D-1-thiogalactopyranoside; ISC, iron–sulfur cluster; LB, Luria–Bertani; NOE, nuclear overhauser effect; OD, optical density; R_1, longitudinal relaxation rate; R_2, transverse relaxation rate; SAXS, small-angle X-ray scattering; SEC-MALS, size exclusion chromatography combined with multiangle light scattering; TCEP, tris (2-carboxyethyl) phosphine.

universally present NFU1 protein [3]. NFU1 was initially thought to be an alternative scaffold to ISCU [4,5], a protein *de novo* assembling Fe-S clusters [6]. Other studies supported a model that NFU1 works in a late step of the mitochondrial ISC assembly machinery transferring a [4Fe-4S] cluster to selected apo target proteins [7,8]. The current prevailing model, largely based on studies in *Saccharomyces cerevisiae* [8], proposes that NFU1 receives a [4Fe-4S] cluster assembled on the ISCAs system and then transfers it to selected apo target proteins with the assistance of BOLA3, another protein of the mitochondrial ISC assembly machinery. This model was supported by the observation of an interaction of yeast NFU1 homologue with both yeast ISCAs homologues and with [4Fe-4S] target proteins, and of an interaction of yeast BOLA3 homologue with the same target proteins of yeast NFU1 homologue [8]. However, the interaction between yeast NFU1 and BOLA3 homologues was not experimentally observed in mitochondrial lysates and not clearly identified in pull-down experiments, being proposed to be transient [8]. Thus, whether and how BOLA3 may facilitate [4Fe-4S] cluster dissociation and transfer from NFU1 to apo target proteins is still unclear. On the other hand, BOLA3 has been found to form a stable dimeric hetero-complex with GLRX5 [9,10], a monothiol glutaredoxin-related component of the mitochondrial ISC assembly machinery that operates upstream in the machinery receiving a $[2Fe\text{-}2S]^{2+}$ cluster assembled on the ISCU scaffold protein [11]. The hetero-dimeric GLRX5-BOLA3 complex is formed both as apo and having a bridged $[2Fe\text{-}2S]^{2+}$ cluster. The $[2Fe\text{-}2S]^{2+}$ GLRX5-BOLA3 hetero-dimeric complex is preferentially formed as hetero-complex with respect to homo-dimeric $[2Fe\text{-}2S]^{2+}$ GLRX5 [9,10]. The proposed functional role of the $[2Fe\text{-}2S]^{2+}$ GLRX5-BOLA3 complex is that of transferring the cluster to apo acceptor(s), although the target(s) need(s) to be identified [10].

While BOLA3 sequence analysis with sorting programs [12,13] uniquely identifies only a mitochondrial isoform, analyses of genomic DNA, transcripts, and translation products indicate that alternative splicing of a common pre-mRNA results in the synthesis of two NFU1 human isoforms with distinct subcellular localizations [5]. Isoform I of NFU1 is localized in the mitochondria and, once processed by mitochondrial processing peptidases has a mature form with a molecular mass of ~ 22 kDa (mNFU1, hereafter), whereas isoform II is present in the cytosol and the nucleus having a molecular mass of ~ 26 kDa [5]. The mitochondrial targeting sequence in mNFU1 is composed by the first 58 residues at the N terminus of the protein [14]. Human mNFU1 is required for the proper assembly of a subset of mitochondrial [4Fe-4S] proteins, which include components of respiratory complexes I and II, and lipoyl synthase [4,7,15]. A recent structural characterization of a construct of human NFU1 42-residue longer at the N terminus than mNFU1 sequence (42-NFU1 hereafter) showed that the apo protein is monomeric in solution and adopts a dumbbell-shaped structure with well-structured N- and C-domains connected by a linker [16]. It has been also shown that chemically Fe-S cluster reconstituted 42-NFU1 binds a [4Fe-4S] cluster [16]. Combined NMR and small-angle X-ray scattering (SAXS) data showed that the holo form is constituted by a trimer of dimers, each containing a [4Fe-4S] cluster [16]. Three N-domains are involved in the formation of a tripartite interface, while two conserved cysteines in the C-domain ligate a [4Fe-4S] cluster to form a dimer by bridging two C-domains.

With the aim of characterizing the molecular function of GLRX5, BOLA3, and mNFU1 in the mitochondrial ISC assembly machinery, we have here first characterized the structure of the holo form of mNFU1 and its interaction with BOLA3 and then investigated the interaction between apo mNFU1 and [2Fe-2S] GLRX5-BOLA3 or [2Fe-2S] GLRX5.

Results

Mitochondrial human NFU1 dimerizes to bind a [4Fe-4S] cluster

The mitochondrial isoform of human NFU1 has a mature state with a molecular mass of ~ 22 kDa, produced after the removal of a N-terminal mitochondrial targeting sequence of 58 residues (mNFU1, hereafter) [5,14]. mNFU1 was isolated from *Escherichia coli* cells in the apo form (see Materials and methods for details). Analytical size exclusion chromatography combined with multiangle light scattering (SEC-MALS) performed on apo mNFU1 showed the presence of a major species eluting with a molar mass of at ~ 22 kDa, corresponding to the monomeric form and of a minor species eluting with a molar mass of 47 kDa (Fig. 1A), which corresponds to a homo-dimeric form of mNFU1. The monomeric and dimeric forms are in equilibrium, whose position almost completely shifts to the monomer upon the increase of the ionic strength to 150 mM NaCl (Fig. 1B). In agreement with this, the reorientational correlation time, estimated from the average ^{15}N transverse relaxation rate (R_2)/longitudinal relaxation rate (R_1) ratios of backbone NHs (Fig. 1C), decreased from 13.5 ± 0.90 ns to 11.8 ± 0.92 ns by addition of 150 mM NaCl. The Brownian rotational

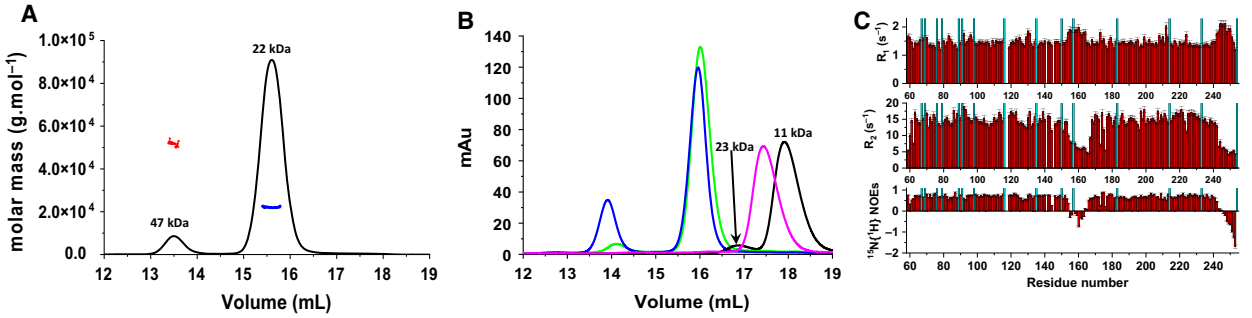

Fig. 1. Monomer-dimer equilibrium and backbone dynamics of apo mNFU1. (A) SEC-MALS profile of apo mNFU1 in phosphate buffer 50 mM pH 7.0, 5 mM DTT, 150 mM NaCl. The red and blue dots indicate the molecular masses in g·mol^{-1} of dimeric and monomeric apo mNFU1, calculated by MALS for each point of the curve. (B) Analytical gel-filtration of apo mNFU1 in phosphate buffer 50 mM pH 7.0, 5 mM DTT with (green) and without (blue) 150 mM NaCl, and of C-domain (magenta) and N-domain (black) of apo mNFU1 in phosphate buffer 50 mM pH 7.0, 150 mM NaCl, 5 mM DTT. (C) ^{15}N R_1, R_2, and heteronuclear ^{15}N[^{1}H] NOEs values (red bars) versus residue number of apo mNFU1 at 298 K in 50 mM phosphate buffer pH 7.0, 5 mM DTT, 150 mM NaCl. Error bars are represented as standard deviation. The cyan bars represent proline residues. The residues whose NHs are not detected or too broad to be analyzed are not shown. SEC-MALS and NMR relaxation experiments were repeated three times.

correlation time value of 10.11 ns calculated for a 24 kDa spherical particle surrounded by a single layer of water [17] is consistent with a globular shape for the ~ 22 kDa mNFU1 molecule, but the present data does not conclusively exclude that some flexibility between the two domains is present. Indeed, eleven backbone NHs of the residues connecting the two domains (i.e., EETPSGEAGSEE, named flexible linker hereafter) show fast backbone motions in the ns-ps time scale experiencing very low or negative heteronuclear ^{15}N [^{1}H] nuclear overhauser effect (NOEs; Fig. 1C). This behavior is typical of highly unstructured and flexible regions and suggests the possible presence of domain-domain flexibility. To investigate whether the two domains interact with each other, we have produced the single N- and C-domains. SEC-MALS data showed that the apo form of the C-domain is fully monomeric in solution, while the N-domain showed the presence of a major species eluting with a molar mass of ~ 11 kDa, corresponding to the monomer, and of a minor species eluting with a molar mass of ~ 23 kDa corresponding to the dimer (Fig. 1B). The ^{1}H-^{15}N heteronuclear single quantum coherence (HSQC) spectra of the N- and C-domains were compared with that of the full-length protein in the presence of 5 mM reduced DTT, to avoid disulfide-linked dimerization as previously observed under oxidizing conditions [16]. Chemical shifts changes were observed on the two α-helices of the C-domain and on the short α-helix, the 3_{10}-helix, and the C terminus of the N-domain (Fig. 2A,B). The flexible linker is required for determining this interaction since, by mixing at 1 : 1 ratio the two single N- and C-domains that do not contain residues 156–161 of the linker, no chemical shifts were observed. In summary, the data indicate that the two domains in the apo mNFU1 monomer, although connected by a flexible linker, are not fully independent. Docking N-domain and C-domain by high ambiguity-driven protein–protein docking (HADDOCK) [18,19] based on chemical shift perturbation data produced a top-scoring cluster of 41 structures out of 200 calculated with a RMSD, from the lowest-energy structure, of 1.1 ± 0.8 Å and a HADDOCK score of −80.0 ± 1.6 (Table 1). The obtained structural model mimics a closed conformational state of monomeric apo mNFU1, but other possible conformations describing the dynamics of the two domains of monomeric mNFU1 are likely present in solution. The best structure, shown in Fig. 2C, indicates that the two domains interact through a hydrophobic patch and a charged patch. These interactions orient the two domains so that the conserved metal-binding CXXC motif, located in the C-domain of mNFU1, is fully exposed to the solvent and can thus be involved in cluster binding (Fig. 2C).

The UV-visible absorption spectrum of the chemically Fe-S cluster reconstituted mNFU1 ([4Fe-4S]$^{2+}$ mNFU1, hereafter, Fig. 3A) showed the presence of a broadband centered at ~ 410 nm, as previously reported [5], which typically dominates the absorption spectra of biological [4Fe-4S]$^{2+}$ clusters [6]. The CD spectrum of [4Fe-4S]$^{2+}$ mNFU1 (Fig. 3B) in the UV-visible region is very weak and featureless, which is also characteristic of biological [4Fe-4S]$^{2+}$ clusters [20]. Moreover, the extinction coefficient at 410 nm of 8.3 mM^{-1}·cm^{-1}, based on the mNFU1 monomeric concentration, is consistent with one [4Fe-4S]$^{2+}$ cluster per mNFU1 dimer [21]. The C-domain of mNFU1 was also chemically Fe-S cluster reconstituted but, in

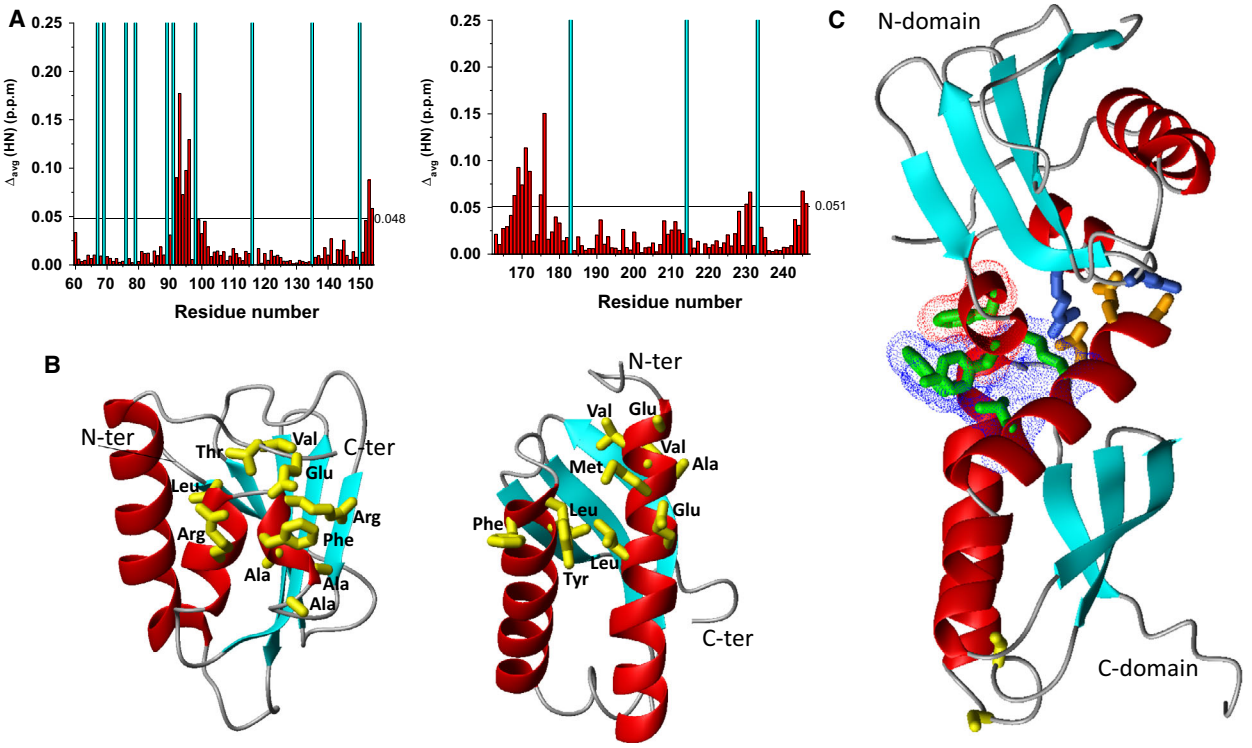

Fig. 2. Structural properties of apo mNFU1. (A) Backbone weighted average chemical shift differences Δ_{avg}(HN) (i.e., $(((\Delta H)^2 + (\Delta N/5)^2)/2)^{1/2}$) (red bars), between full-length apo mNFU1 and the N-domain (left panel) or apo C-domain (right panel) of mNFU1. The indicated threshold values (obtained by averaging Δ_{avg}(HN) values plus 1σ) were used to define meaningful chemical shift differences. The cyan bars represent proline residues. (B) The side chains of the residues experiencing meaningful chemical shift differences were mapped as yellow sticks on the solution structures of N- and apo C-domains [16]. (C) Theoretical modeling of N-domain docking to apo C-domain of mNFU1 using HADDOCK program. Hydrophobic residues on both structures are in green, and their contact surfaces are as dotted areas in red and blue on N-domain and apo C-domain, respectively. Positively charged residues, Arg and Lys, and negatively charged residues, Asp and Glu, are in blue and orange, respectively. Cysteines of the conserved CXXC motif are in yellow. NMR experiments were repeated three times. The models shown in panels B and C were rendered with MOLMOL molecular graphics program.

all tested conditions, no more than ~ 50% of $[4Fe\text{-}4S]^{2+}$ loaded mNFU1 was obtained, demonstrating that the N-domain is essential to obtain a quantitative cluster binding on the C-domain. ^{15}N heteronuclear NMR relaxation measurements on $[4Fe\text{-}4S]^{2+}$ mNFU1 (Fig. 3C) provided a reorientational correlation time of 15.1 ± 1.2 ns, increased with respect to the value of 11.8 ns estimated for apo mNFU1, in agreement with protein dimerization. The heteronuclear $^{15}N[^1H]$ NOEs of the flexible linker are still negative in $[4Fe\text{-}4S]^{2+}$ mNFU1, indicating that the linker conserves its flexibility in the holo form (Fig. 3C). The comparison of the $^1H\text{-}^{15}N$ HSQC spectrum of $[4Fe\text{-}4S]^{2+}$ mNFU1 with that of apo mNFU1 revealed that the Fe-S cluster binding led to large chemical shift perturbations and significant line broadening (Fig. 4A). Only one set of peaks for each residue was observed in the $^1H\text{-}^{15}N$ HSQC spectrum of $[4Fe\text{-}4S]^{2+}$ mNFU1, as it occurs in the $^1H\text{-}^{15}N$ HSQC spectrum of apo mNFU1 (Fig. 4A), indicating the presence of a symmetric holo dimer. Chemical shift perturbations were observed on both N- and C-domains. Specifically, while the N-domain shows only chemical shift changes, the C-domain shows also line broadening effects beyond detection for eleven backbone NHs of the region containing the conserved CXXC motif. These broadening effects are a consequence of the binding of the paramagnetic [4Fe-4S] cluster to the cysteines of the CXXC motif. The peaks of the N-domain in the $^1H\text{-}^{15}N$ HSQC spectrum of $[4Fe\text{-}4S]^{2+}$ mNFU1 do not match with those of the single N-domain of mNFU1, suggesting that the N-domain is not fully independent to move in solution in $[4Fe\text{-}4S]^{2+}$ mNFU1 (Fig. 4B). In summary, these data indicate that the cluster is bridged between two C-domains in the symmetric dimer and is coordinated by two CXXC motifs from each subunit of the dimer. On the contrary, the N-domain is not directly involved in cluster binding and the chemical shift changes observed on its residues upon cluster binding reflect a change of the intramolecular contacts between the N- and C-domains.

Table 1. Statistics of the HADDOCK docking run for the first three best-scoring clusters by docking N-domain and C-domain of mNFU1

	Cluster 1	Cluster 2	Cluster 3
HADDOCK score	−80.0 ± 1.6	−65.8 ± 5.2	−55.4 ± 2.0
Cluster size	41	18	49
RMSD from the overall lowest-energy structure	1.1 ± 0.8	5.7 ± 0.7	4.7 ± 1.3
Van der Waals energy	−26.4 ± 4.4	−21.3 ± 4.8	−16.2 ± 2.4
Electrostatic energy	−240.7 ± 49.1	−184.3 ± 30.0	−133.2 ± 25.8
Desolvation energy	−9.9 ± 6.3	−8.5 ± 5.1	13.1 ± 4.5
Restraints violation energy	44.6 ± 16.6	9.1 ± 1.88	4.5 ± 2.03
Buried surface area	911.1 ± 47.4	900.5 ± 63.2	721.6 ± 49.4
Z-score	−2.0	−0.8	0.1

The paramagnetic 1D ^{1}H NMR spectrum of [4Fe-4S]$^{2+}$ mNFU1 showed the presence of two close hyperfine-shifted signals at 20.2 and 19.5 p.p.m. and one at 12.7 p.p.m. (Fig. 4Ca), all showing an anti-Curie temperature dependence. The chemical shift values of these signals, their anti-Curie temperature dependence, and their linewidths are typical of βCH_2 signals of Cys residues bound to a [4Fe-4S]$^{2+}$ cluster with an S = 0 electronic ground state, with the paramagnetism arising from excited states of the electron spin ladder, partially populated at room temperature [22]. By adding 5 mM reduced glutathione (GSH) to [4Fe-4S]$^{2+}$ mNFU1, the 1D ^{1}H paramagnetic NMR spectrum changes showing the presence of three further hyperfine-shifted signals at 15.5, 13.5, and 11.3 p.p.m. (Fig. 4Cb), indicating that GSH modifies the coordination environment, possibly acting as a ligand with its Cys residue. Nevertheless, GSH does not fully replace the Cys protein ligand since the three signals at 20.2, 19.5, 12.7 p.p.m. are still present (Fig. 4Cb). A mixture of at least two [4Fe-4S]$^{2+}$ species is present, most likely one derived from all protein-derived Cys protein ligands and the other from a GSH ligand and three protein-derived Cys ligands. Analyzing the interaction between apo mNFU1 and GSH through ^{1}H-^{15}N HSQC experiments, it appears that the chemical shifts of the backbone NH signals of Cys 213, Ser 215, Ser 216, Ile 217, Ile 218, Leu 220, that include and surround the CXXC motif, change upon the addition of GSH (Fig. 5A). The solution NMR structure of the C-domain of mNFU1 in its apo form [16] showed that Cys 213 ligand is more solvent-exposed than the other cysteine ligand, that is, Cys 210 (Fig. 5B). Our NMR data thus indicate that GSH interacts with the region close to the solvent-exposed Cys 213, suggesting that this cysteine is the ligand preferentially displaced by GSH in [4Fe-4S]$^{2+}$ mNFU1 (Fig. 5B). Upon addition of 5 mM DTT to the 5 mM GSH/[4Fe-4S]$^{2+}$ mNFU1 mixture, the 1D ^{1}H paramagnetic NMR spectrum showed further changes. The three signals at 20.2, 19.5, 12.7 p.p.m. of the DTT- and GSH-free protein as well as the three signals of the GSH-bound form disappeared, and three new signals at 20.3, 14.5, and 13.6 p.p.m. appear, all displaying an anti-Curie temperature dependence (Fig. 4Cc). The size and the anti-Curie temperature dependence of the chemical shifts of these signals indicate that a [4Fe-4S]$^{2+}$ cluster with an S = 0 electronic ground state is still bound to mNFU1 in the presence of DTT, but the change observed in

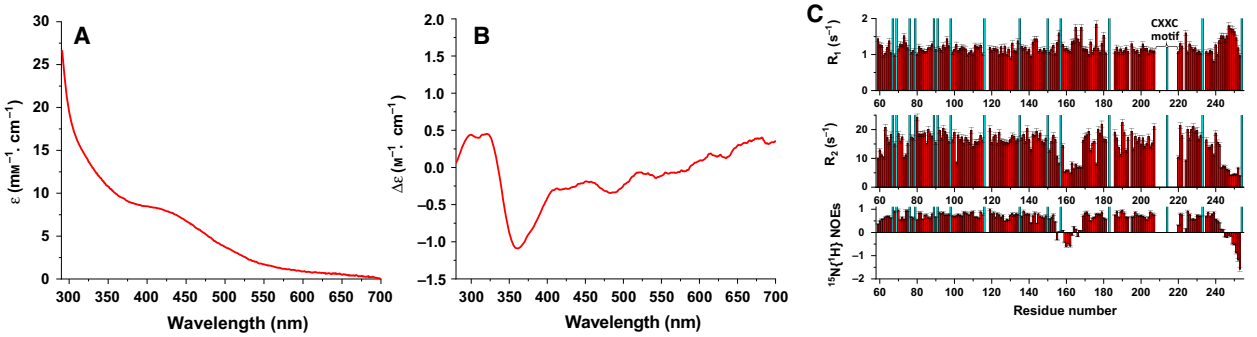

Fig. 3. UV-visible absorption spectroscopy and backbone dynamics on chemically reconstituted [4Fe-4S]$^{2+}$ mNFU1. UV-visible (A) and CD-visible (B) spectra of [4Fe-4S]$^{2+}$ mNFU1 in 50 mM phosphate buffer pH 7.0, 5 mM DTT, 150 mM NaCl. (C) ^{15}N R_1, R_2 and heteronuclear ^{15}N [^{1}H] NOEs values (red bars) versus residue number of [4Fe-4S]$^{2+}$ mNFU1 at 298 K in 50 mM phosphate buffer pH 7.0, 5 mM DTT, 150 mM NaCl. The cyan bars represent proline residues. The residues whose NHs are not detected or too broad to be analyzed are not shown. UV-vis, CD, and NMR relaxation experiments were repeated three times.

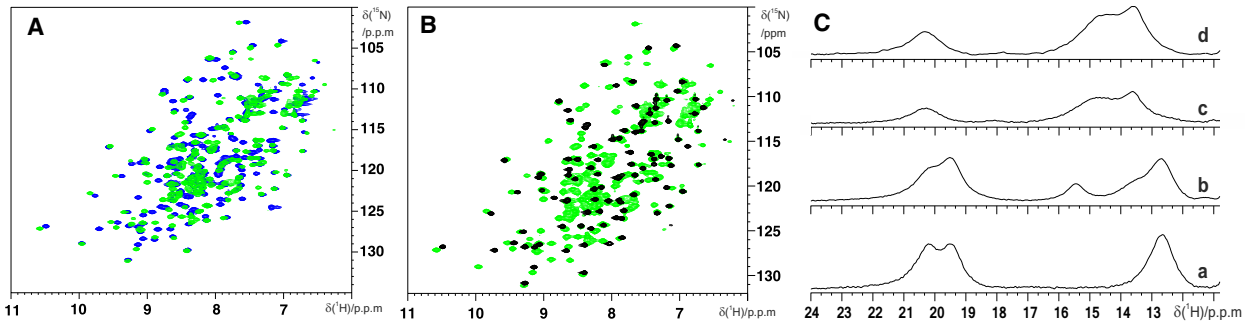

Fig. 4. NMR characterization of $[4Fe\text{-}4S]^{2+}$ mNFU1. (A) Overlay of $^{1}H\text{-}^{15}N$ HSQC spectra of apo (blue) and $[4Fe\text{-}4S]^{2+}$ (green) mNFU1, acquired at 298 K in 50 mM phosphate buffer pH 7.0, 5 mM DTT, 150 mM NaCl. (B) Overlay of $^{1}H\text{-}^{15}N$ HSQC spectra of $[4Fe\text{-}4S]^{2+}$ mNFU1 (green) and of the N-domain of mNFU1 (black), acquired at 298 K in 50 mM phosphate buffer pH 7.0, 5 mM DTT, 150 mM NaCl. (C) 1D ^{1}H NMR spectra tailored for the detection of hyperfine-shifted signals of $[4Fe\text{-}4S]^{2+}$ mNFU1 were acquired at 298 K in 50 mM phosphate buffer pH 7.0, 150 mM NaCl (a), and upon sequential additions of 5 mM GSH (b) and 5 mM DTT to the same protein sample (c), and of $[4Fe\text{-}4S]^{2+}$ mNFU1 acquired in the presence of 5 mM DTT alone. NMR experiments were repeated three times.

their pattern indicates a modified cluster coordination, where DTT acts as a cluster ligand and fully displaces GSH from coordination. In agreement with this interpretation of the NMR data, the paramagnetic 1D ^{1}H NMR spectrum of $[4Fe\text{-}4S]^{2+}$ mNFU1 acquired in the presence of 5 mM DTT alone (i.e., sample never treated with GSH) is perfectly superimposable with that acquired in the presence of 5 mM GSH and 5 mM DTT (Fig. 4Cd), confirming that DTT fully displaced GSH in the coordination sphere of the cluster.

The $^{1}H\text{-}^{15}N$ HSQC spectra acquired on $[4Fe\text{-}4S]^{2+}$ mNFU1 in the presence of DTT (or GSH) are also different from that of DTT-free (or GSH-free) $[4Fe\text{-}4S]^{2+}$ mNFU1 but the observed resonances do not have the chemical shifts of apo mNFU1 (Fig. 6A). This result agrees with the model that GSH and DTT are unable to displace a mNFU1 molecule from the holo dimer to form a monomeric $[4Fe\text{-}4S]^{2+}$ mNFU1 species where two GSH or DTT molecules bind to the cluster. In such a case, the appearance of peaks corresponding to an apo mNFU1 molecule released from the holo dimer would be indeed expected in the $^{1}H\text{-}^{15}N$ HSQC spectrum of the DTT (or GSH)/$[4Fe\text{-}4S]^{2+}$ mNFU1 mixture. Finally, 1D ^{1}H paramagnetic or $^{1}H\text{-}^{15}N$ HSQC NMR spectra (Figs 6B and 5A), acquired on $[4Fe\text{-}4S]^{2+}$ mNFU1 treated first with GSH (or DTT) or and then passed on a PD-10 desalting column, are the same as that of the GSH-free (or DTT-free) $[4Fe\text{-}4S]^{2+}$ mNFU1, indicating that the DTT and GSH molecules initially bound to the cluster are then removed from the cluster coordination, due to an equilibrium between GSH/DTT-bound holo protein and free GSH/DTT holo protein.

BOLA3 drives the [4Fe-4S] cluster assembly on mNFU1

Considering the proposed model that a mNFU1-BOLA3 complex mediates the transfer of a [4Fe-4S] cluster from ISCA complex to apo target proteins [8],

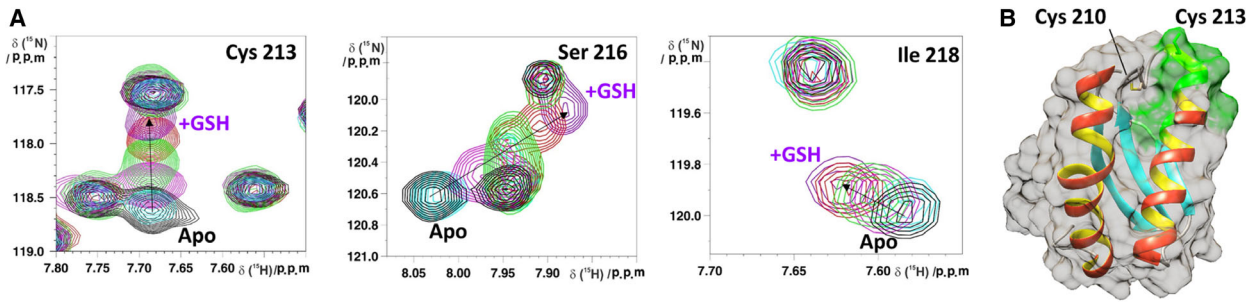

Fig. 5. Monitoring the interaction between GSH and apo mNFU1 by NMR. (A) Overlay of $^{1}H\text{-}^{15}N$ HSQC spectra of apo ^{15}N-labeled mNFU1, acquired at 298 K in 50 mM phosphate buffer pH 7.0, 150 mM NaCl, in the absence (black) and in the presence of increasing concentrations of GSH up to 7 mM (from black to violet). The final mixture was exchanged in the original buffer in the absence of GSH (cyan). (B) Mapping the chemical shift changes (shown in green) on the C-domain of mNFU1 (PDB ID 2M5O) occurring upon the interaction between apo mNFU1 and GSH. NMR experiments were repeated three times. The model shown in panel 5B was rendered with UCSF Chimera.

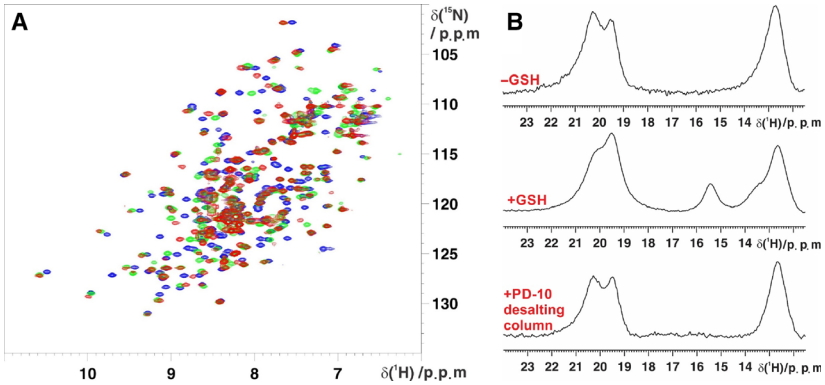

Fig. 6. DTT does not promote the formation of apo mNFU1 by its addition to $[4Fe\text{-}4S]^{2+}$ mNFU1 and GSH-binding equilibrium in $[4Fe\text{-}4S]^{2+}$ mNFU1. (A) Overlay of ^{1}H-^{15}N HSQC spectra of ^{15}N-labeled $[4Fe\text{-}4S]^{2+}$ mNFU1 in the presence (green) and in the absence (red) of 5 mM DTT with that of ^{15}N-labeled apo mNFU1 (blue) in the presence of 5 mM DTT, acquired at 298 K in 50 mM phosphate buffer pH 7.0, 150 mM NaCl. (B) 1D ^{1}H NMR spectra tailored for the detection of hyperfine-shifted signals of $[4Fe\text{-}4S]^{2+}$ mNFU1 in the absence of GSH (upper), in the presence of 5 mM GSH (middle) and after exchanging, through PD-10 desalting column, the latter mixture in the same buffer but not containing GSH. NMR spectra were acquired at 298 K in 50 mM phosphate buffer pH 7.0 and 150 mM NaCl. NMR experiments were repeated two times.

we have investigated, by NMR, UV-visible and CD spectroscopy, the potential interaction between BOLA3 and mNFU1. NMR titration experiments on ^{15}N-labeled samples showed that apo NFU1 does not interact with BOLA3 (Fig. 7A,B). To characterize the potential interaction between BOLA3 and mNFU1 in the presence of a Fe-S cluster, we have performed a chemical reconstitution with iron and sulfide ions on a mixture composed by apo mNFU1 and BOLA3 in various experimental conditions (see Experimental Section for details) and spectroscopically characterized it. In all cases, the UV-visible and CD spectra are essentially identical to the spectra of $[4Fe\text{-}4S]^{2+}$ mNFU1 (Fig. 8A,B), suggesting that BOLA3 does not modify the Fe-S cluster nuclearity. Consistently, the ^{1}H 1D paramagnetic NMR spectrum of the chemically reconstituted mixture is typical of that of $[4Fe\text{-}4S]^{2+}$ mNFU1 (Fig. 8C), indicating that BOLA3 does not contribute to the cluster binding. Comparison of the ^{1}H-^{15}N HSQC NMR spectra of the chemically reconstituted mixture with those of the isolated proteins showed that the two proteins do not interact each other since no significant chemical shift changes occurred and that only a $[4Fe\text{-}4S]^{2+}$ mNFU1 species is formed in the chemical Fe-S cluster reconstitution process (Fig. 7C,D). We also tested the potential interaction between BOLA3 and $[4Fe\text{-}4S]^{2+}$ NFU1 in the presence of GLRX5 by performing a NMR titration experiment where unlabeled $[4Fe\text{-}4S]^{2+}$ mNFU1 was added to a 1 : 1 mixture of ^{15}N-labeled BOLA3 and unlabeled apo GLRX5. The results showed that the apo protein complex formed between GLRX5 and BOLA3 [9,10] does not interact with $[4Fe\text{-}4S]^{2+}$ mNFU1 (Fig. 7E). In conclusion, we can rule out any possible interaction of BOLA3 with either apo or $[4Fe\text{-}4S]^{2+}$ mNFU1 in the absence and in the presence of GLRX5.

The latter results brought us to investigate a different pathway through which BOLA3 and mNFU1 can cooperate in assisting the formation of a [4Fe-4S] cluster on apo target proteins. Since it has been already shown that BOLA3 and GLRX5 form a heterodimeric complex able to bind a $[2Fe\text{-}2S]^{2+}$ cluster [9,10], we investigated whether this complex can interact with apo mNFU1, transfer the cluster, and form a [4Fe-4S] cluster on mNFU1. We followed these possible processes by NMR, UV-visible, and CD spectroscopy. The experiments were performed by adding either apo mNFU1 to the $[2Fe\text{-}2S]^{2+}$ GLRX5-BOLA3 hetero-complex or vice versa, and, for NMR measurements, ^{15}N-labeling one protein at a time or ^{15}N-labeling two out of the three proteins. Comparing the UV-visible spectrum of the $[2Fe\text{-}2S]^{2+}$ GLRX5-BOLA3 hetero-complex with those of two mixtures containing different ratios of $[2Fe\text{-}2S]^{2+}$ GLRX5-BOLA3 and apo mNFU1, significant changes of the absorption bands were observed (Fig. 9A). In particular, the bands characteristic of the $[2Fe\text{-}2S]^{2+}$ cluster bound to GLRX5-BOLA3 complex decrease in intensity and the final spectrum resembles to that of $[4Fe\text{-}4S]^{2+}$ mNFU1 (Fig. 9A). The same mixtures, analyzed by CD spectroscopy, showed a loss of intensity of the CD signals of the $[2Fe\text{-}2S]^{2+}$ GLRX5-BOLA3 hetero-complex, suggesting the formation of $[4Fe\text{-}4S]^{2+}$ mNFU1, whose CD signals are indeed very low in intensity (Fig. 9B) [20,23]. In the NMR titration between the $[2Fe\text{-}2S]^{2+}$

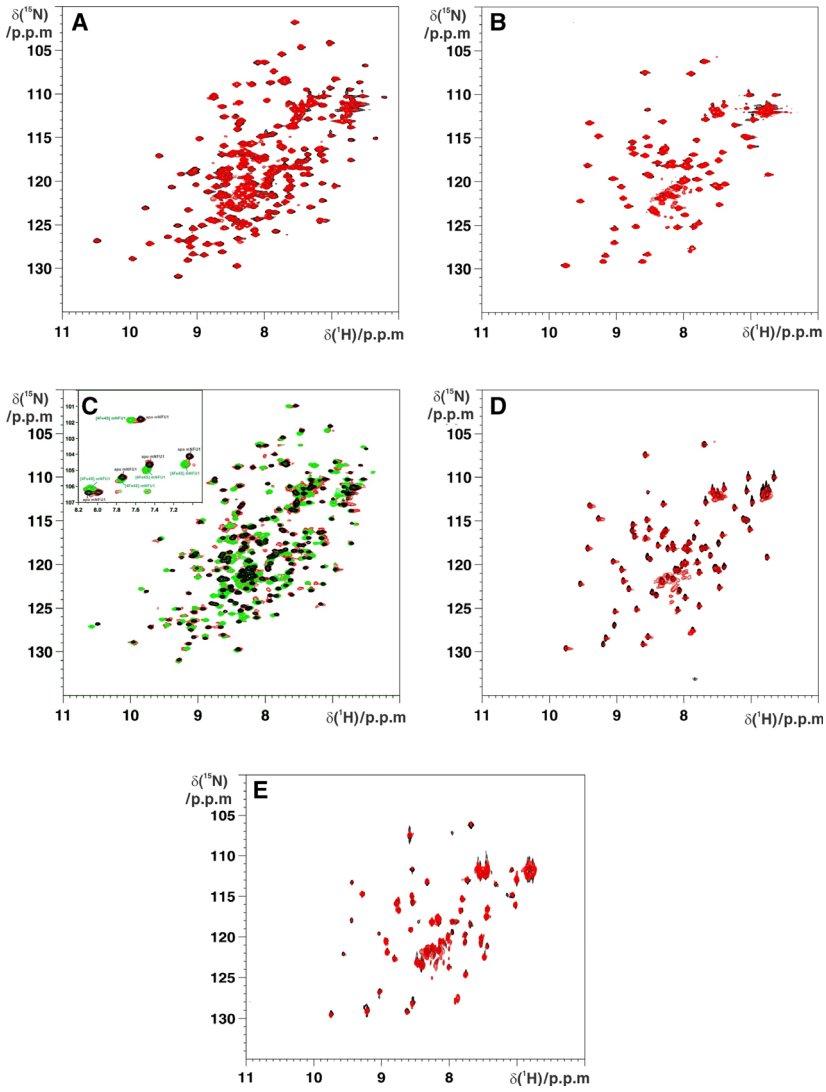

Fig. 7. BOLA3 does not interact with mNFU1. Overlay of ^{1}H-^{15}N HSQC NMR spectra of (A) ^{15}N-labeled apo mNFU1 (black) and a 1 : 1 mixture of ^{15}N-labeled apo mNFU1 and unlabeled BOLA3 (red); (B) ^{15}N-labeled BOLA3 (black) and a 1 : 1 mixture of ^{15}N-labeled BOLA3 and unlabeled apo mNFU1 (red); (C) ^{15}N-labeled apo mNFU1 (black), ^{15}N-labeled $[4Fe\text{-}4S]^{2+}$ mNFU1 (green) and a chemically Fe-S cluster reconstituted 2 : 1 mixture of unlabeled BOLA3 and ^{15}N-labeled apo mNFU1 (red); (D) ^{15}N-labeled BOLA3 (black) and a chemically Fe-S cluster reconstituted 1 : 1 mixture of ^{15}N-labeled BOLA3 and unlabeled apo mNFU1 (red); (E) apo ^{15}N-labeled BOLA3-unlabeled GLRX5 hetero-complex (black) and a 1 : 1 mixture of apo ^{15}N-labeled BOLA3-unlabeled GLRX5 hetero-complex and unlabeled $[4Fe\text{-}4S]^{2+}$ mNFU1 (red), both in the presence of 5 mM GSH. NMR spectra were acquired at 298 K in 50 mM phosphate buffer pH 7.0, 5 mM DTT and 150 mM NaCl. NMR experiments were repeated three times.

^{15}N-labeled GLRX5-unlabeled BOLA3 complex and unlabeled apo mNFU1, the resonances of the $[2Fe\text{-}2S]^{2+}$ GLRX5-BOLA3 hetero-complex disappeared and concomitantly the resonances of the apo GLRX5-BOLA3 hetero-complex appeared (Fig. 9D), indicating the cluster release from the hetero-complex. In the titration between the unlabeled $[2Fe\text{-}2S]^{2+}$ GLRX5-^{15}N-labeled BOLA3 complex and ^{15}N-labeled apo mNFU1, the changes observed for the BOLA3 resonances indicate again the occurrence of cluster release from the hetero-complex (Fig. 9E). Concomitantly, the new resonances appearing in the ^{1}H-^{15}N HSQC map of the mixture have chemical shifts matching with those of $[4Fe\text{-}4S]^{2+}$ mNFU1, indicating the formation of $[4Fe\text{-}4S]^{2+}$ mNFU1 (Fig. 9F). In agreement with the latter data, the 1D ^{1}H paramagnetic NMR spectrum acquired on the final mixture showed the presence of the typical peaks of $[4Fe\text{-}4S]^{2+}$ mNFU1 (Fig. 9C). Overall, the experimental data indicate the transfer of two $[2Fe\text{-}2S]^{2+}$ clusters from the $[2Fe\text{-}2S]^{2+}$ GLRX5-BOLA3 hetero-complex to apo mNFU1 and the concomitant formation of a $[4Fe\text{-}4S]^{2+}$ cluster. A reducing agent is absolutely required for converting ferric ions present in the $[2Fe\text{-}2S]^{2+}$ cluster into a mixture of ferric and ferrous ions in the $[4Fe\text{-}4S]^{2+}$ cluster (reductive coupling reaction) [23–25]. Considering that 5 mM DTT and 5 mM GSH were present in all protein mixtures, these two small molecules are the best candidates to act as reducing agents. To verify this hypothesis, the same experiment reported above was performed in the absence of DTT, that is, the $[2Fe\text{-}2S]^{2+}$ unlabeled GLRX5-^{15}N-labeled BOLA3 complex mixed with ^{15}N-labeled apo mNFU1. In this case, we observed that the reaction did not proceed, that is, no

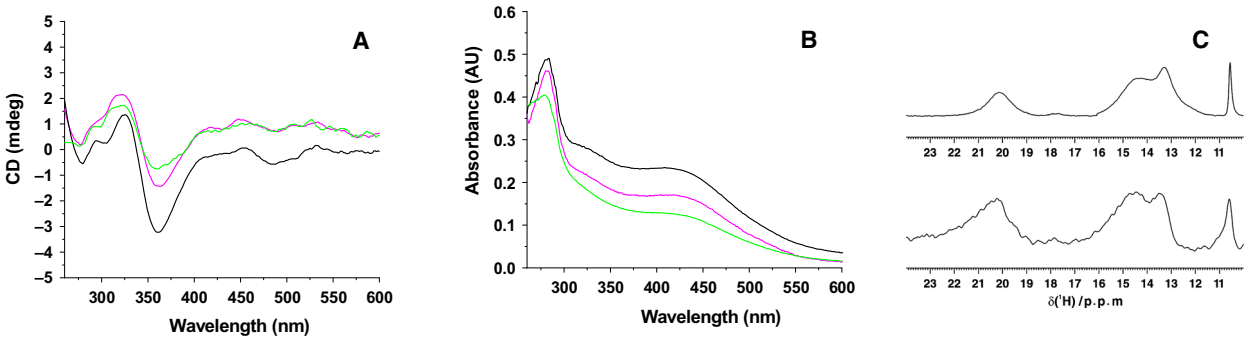

Fig. 8. BOLA3 does not modify cluster binding properties of mNFU1. UV-visible (A) and CD-visible (B) spectra of chemically reconstituted mixtures of BOLA3 and mNFU1: magenta, chemical reconstitution of BOLA3 : mNFU1 at a 1 : 1 ratio in the presence of 5 mM GSH, 5 mM DTT, and 150 mM NaCl; black, chemical reconstitution of BOLA3 : mNFU1 at a 1 : 1 ratio in the presence of 5 mM DTT and 150 mM NaCl. In green are the UV-visible and visible CD spectra of $[4Fe\text{-}4S]^{2+}$ mNFU1. (C) 1D ^{1}H NMR spectra tailored for the detection of hyperfine-shifted signals of $[4Fe\text{-}4S]^{2+}$ mNFU1 (upper) and of the chemically reconstituted 1 : 1 BOLA3:mNFU1 mixture (lower). NMR spectra were acquired at 298 K in 50 mM phosphate buffer pH 7.0, 5 mM DTT, and 150 mM NaCl. UV-vis, CD, and NMR experiments were repeated three times.

$[2Fe\text{-}2S]^{2+}$ cluster transfer occurred nor $[4Fe\text{-}4S]^{2+}$ cluster was formed. Indeed, the $^{1}H\text{-}^{15}N$ HSQC spectrum of the mixture is superimposable with those of the individual proteins and no peaks of the $[4Fe\text{-}4S]^{2+}$ mNFU1 product are formed (Fig. 10). DTT is therefore the reducing agent *in vitro* required for the reductive coupling reaction to occur. DTT is, however, not an efficient reducing system. Indeed, DTT is not able to quantitatively form the $[4Fe\text{-}4S]^{2+}$ mNFU1 product in the 1 : 1 $[2Fe\text{-}2S]^{2+}$ GLRX5-BOLA3/apo mNFU1 mixture, being the amount of $[4Fe\text{-}4S]^{2+}$ mNFU1 65% (estimated from $^{1}H\text{-}^{15}N$ HSQC NMR data, see Fig. 8F). Even when an excess of two equivalents of $[2Fe\text{-}2S]^{2+}$ GLRX5-BOLA3 was added to apo mNFU1, the resonances associated with apo mNFU1 do not disappear completely. Moreover, the formation of $[4Fe\text{-}4S]^{2+}$ mNFU1 occurs slowly upon time in the presence of 5 mM DTT, that is, it reaches the equilibrium only after 1 day. Overall, from these data we can gather that a physiological electron donor is required to efficiently promote $[4Fe\text{-}4S]^{2+}$ cluster formation on mNFU1. The best candidate physiological electron donor might be a ferredoxin, a versatile protein family typically involved in electron transfer in mitochondria [26]. Human mitochondria possess two mitochondrial ferredoxins, which are both present in the matrix of mitochondria and have been shown to be versatile electron mediators involved in multiple physiological processes such as Fe-S cluster biogenesis, steroidogenesis, vitamin D metabolism, and heme A biosynthesis [26–28].

We have finally observed by NMR and UV-visible spectroscopy that, when apo or $[2Fe\text{-}2S]^{2+}$ GLRX5 was mixed with apo mNFU1 using DTT as electron source, no protein–protein interaction, no cluster transfer from GLRX5 to mNFU1, and no formation of a $[4Fe\text{-}4S]^{2+}$ cluster on mNFU1 occurred (Fig. 11). This indicates that both cluster transfer and reductive coupling reactions encompassing mNFU1 require BOLA3 to occur. Thus, BOLA3 acts as a trigger factor activating cluster transfer and assembly on mNFU1.

Discussion

The late stages of the mitochondrial ISC assembly machinery are responsible of [4Fe-4S] cluster assembly, trafficking, and insertion into mitochondrial target Fe-S proteins [1,2]. The first studies on the mitochondrial [4Fe-4S] cluster assembly step showed that three human proteins ISCA1, ISCA2, and IBA57 are required for this process [29]. This functional association has been revisited in a recent work [30], which showed that ISCA2 and IBA57 are not required under standard physiological conditions for the maturation of mitochondrial [4Fe-4S] proteins. Therefore, the so far available *in vivo* data do not provide a clear picture on how the three proteins operate in the cell for assembling a [4Fe-4S] cluster. *In vitro* experiments helped to shed some light on this issue showing that (a) ISCA1 and ISCA2 form a hetero-dimer, which, by accepting two $[2Fe\text{-}2S]^{2+}$ clusters from the protein partner GLRX5 (component of the mitochondrial ISC assembly machinery receiving the $[2Fe\text{-}2S]^{2+}$ cluster from ISCU), is able to assemble a $[4Fe\text{-}4S]^{2+}$ cluster, without any need of IBA57 [25,31]; (b) ISCA2, but not ISCA1, after having received a $[2Fe\text{-}2S]^{2+}$ cluster from GLRX5, forms a $[2Fe\text{-}2S]^{2+}$-bridged hetero-dimeric

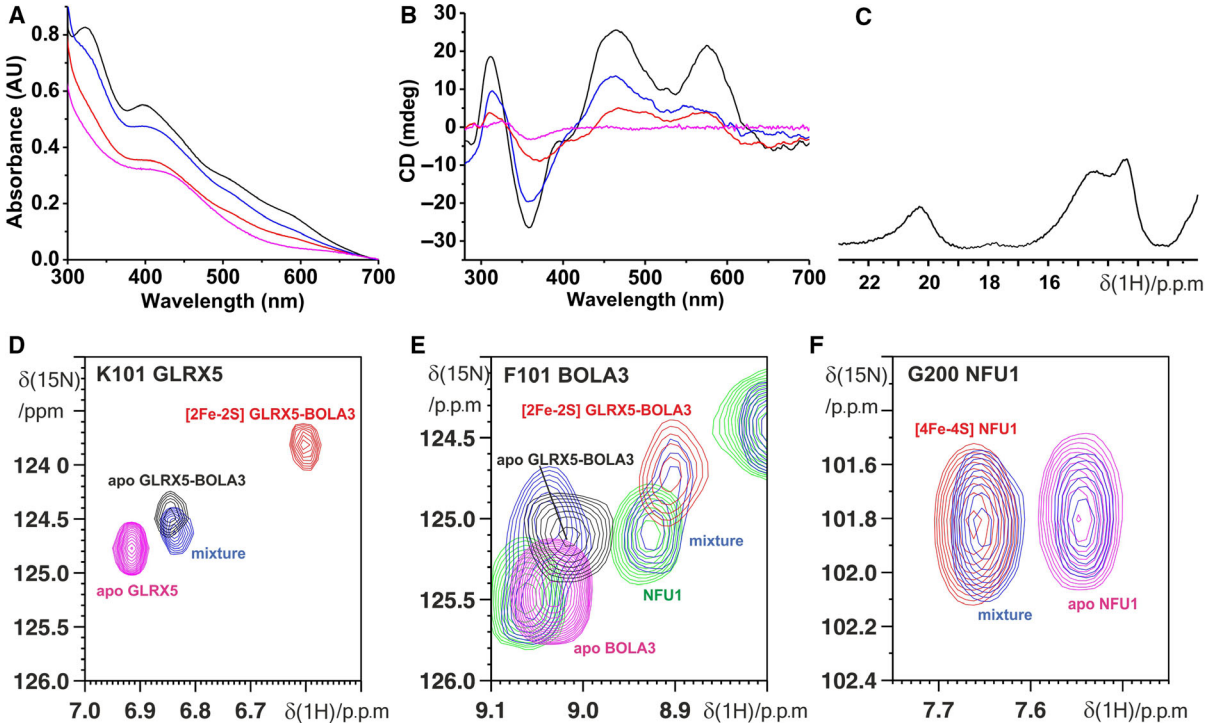

Fig. 9. $[2Fe\text{-}2S]^{2+}$ GLRX5-BOLA3 assembles a $[4Fe\text{-}4S]^{2+}$ cluster on mNFU1. UV-visible (A) and CD (B) spectra of 0.5 : 1 (blue) and 1 : 1 (red) mixtures of $[2Fe\text{-}2S]^{2+}$ GLRX5-BOLA3 hetero-complex and apo mNFU1, compared with spectra of $[2Fe\text{-}2S]^{2+}$ GLRX5-BOLA3 (black) and $[4Fe\text{-}4S]^{2+}$ mNFU1 (magenta). (C) 1D ^{1}H NMR spectra of the hyperfine-shifted signals of the 1 : 1 mixture of $[2Fe\text{-}2S]^{2+}$ GLRX5-BOLA3 hetero-complex and apo mNFU1. Overlay of $^{1}H\text{-}^{15}N$ HSQC NMR spectra of (D) the 1 : 1 mixture of $[2Fe\text{-}2S]^{2+}$ ^{15}N-labeled GLRX5-unlabeled BOLA3 hetero-complex and unlabeled apo mNFU1 (blue), $[2Fe\text{-}2S]^{2+}$ ^{15}N-labeled GLRX5-unlabeled BOLA3 (red), apo ^{15}N-labeled GLRX5-unlabeled BOLA3 (black) and apo ^{15}N-labeled GLRX5 (fuchsia); (E) the 1 : 1 mixture of $[2Fe\text{-}2S]^{2+}$ unlabeled GLRX5-^{15}N-labeled BOLA3 hetero-complex and apo ^{15}N-labeled mNFU1 (blue), $[2Fe\text{-}2S]^{2+}$ unlabeled GLRX5-^{15}N-labeled BOLA3 (red), apo unlabeled GLRX5-^{15}N-labeled BOLA3 (black), apo ^{15}N-labeled BOLA3 (fuchsia), and $[4Fe\text{-}4S]^{2+}$/apo ^{15}N-labeled mNFU1 (green); (F) the 1 : 1 mixture of $[2Fe\text{-}2S]^{2+}$ unlabeled GLRX5-unlabeled BOLA3 hetero-complex and apo ^{15}N-labeled mNFU1 (blue), $[4Fe\text{-}4S]^{2+}$ ^{15}N-labeled mNFU1 (red) and apo ^{15}N-labeled mNFU1 (fuchsia). All spectra were acquired at 298 K in 50 mM phosphate buffer pH 7.0, 5 mM GSH, 5 mM DTT, 150 mM NaCl. UV-vis, CD, and NMR experiments were repeated three times.

complex with IBA57, which results resistant to highly oxidative environments and capable of reactivating apo aconitase [32]. In conclusion, the *in vitro* studies suggested a model of $[4Fe\text{-}4S]^{2+}$ cluster assembly on the ISCA1-ISCA2 complex, while IBA57 might be involved with GLRX5 and ISCA2 in a specific pathway maturing Fe-S proteins under oxidative metabolism. The proposed following step of the mitochondrial ISC assembly machinery consists of the transfer and insertion of the $[4Fe\text{-}4S]^{2+}$ cluster assembled on the ISCA1-ISCA2 complex into mitochondrial target Fe-S proteins with the help of specific ISC targeting factors [1,2]. Two proteins, that is, BOLA3 and NFU1, have been proposed to be involved in this step. NFU1 was implicated in receiving the cluster from the ISCA1-ISCA2 complex [4,7], and BOLA3 was proposed to mediate the transfer of the $[4Fe\text{-}4S]^{2+}$ cluster bound to NFU1 into specific mitochondrial target proteins [8]. However, the interaction between NFU1 and BOLA3 was not clearly detected *in vivo* and it was proposed to be transient [8]. On the contrary, the interaction between BOLA3 and GLRX5 has been well documented by *in vivo* studies [33], and *in vitro* studies recently showed that BOLA3 strongly binds GLRX5, while the binding of BOLA3 to NFU1 is weak [34]. As mentioned above, GLRX5 acts in the early-acting steps of the mitochondrial ISC assembly machinery donating its $[2Fe\text{-}2S]^{2+}$ cluster to the ISCA1-ISCA2 complex [11,25]. Therefore, the raising question is whether GLRX5 has a further role as $[2Fe\text{-}2S]^{2+}$ cluster trafficking protein in the late stages of the mitochondrial ISC assembly machinery once complexed with BOLA3. Our work sheds light on this question, showing that two $[2Fe\text{-}2S]^{2+}$ GLRX5-BOLA3 complexes are able to transfer their clusters to apo NFU1 to form a $[4Fe\text{-}4S]^{2+}$ cluster on dimeric

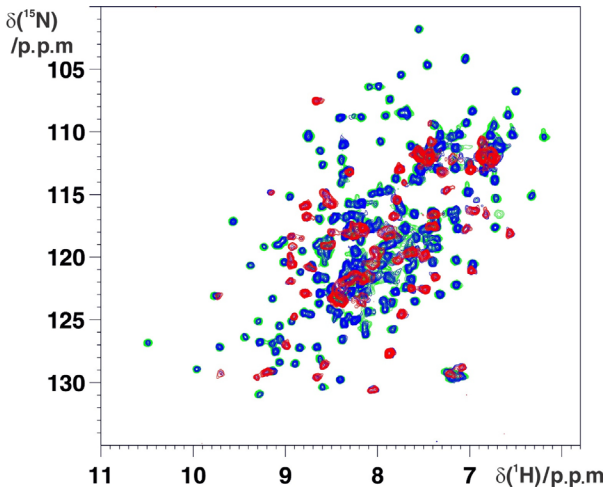

Fig. 10. A reductant is required to assemble a $[4Fe\text{-}4S]^{2+}$ cluster on mNFU1 upon the interaction with the cluster donor $[2Fe\text{-}2S]^{2+}$ GLRX5-BOLA3. Overlay of ^{1}H-^{15}N HSQC NMR spectra of $[2Fe\text{-}2S]^{2+}$ unlabeled GLRX5-^{15}N-labeled BOLA3 (red), apo ^{15}N-labeled mNFU1 (green), and a 1 : 1 mixture of $[2Fe\text{-}2S]^{2+}$ unlabeled GLRX5-^{15}N-labeled BOLA3 and apo ^{15}N-labeled mNFU1 (blue), acquired at 298 K in 50 mM phosphate buffer pH 7.0, 5 mM GSH, and 150 mM NaCl. NMR experiments were repeated three times.

NFU1 (Fig. 12). Our data showed that the mechanism for cluster transfer and assembly from $[2Fe\text{-}2S]^{2+}$ GLRX5-BOLA3 to NFU1 leads directly to the formation of $[4Fe\text{-}4S]^{2+}$ NFU1 without the accumulation of [2Fe-2S]-bound intermediates, in support of a strong preference of NFU1 to bind a [4Fe-4S] cluster with respect to a [2Fe-2S] cluster. The cluster formation on NFU1 does not occur with $[2Fe\text{-}2S]^{2+}$ GLRX5 alone, thus this pathway being activated only upon the formation of the $[2Fe\text{-}2S]^{2+}$ GLRX5-BOLA3 hetero-complex (Fig. 12). Therefore, homo-dimeric $[2Fe\text{-}2S]^{2+}$ GLRX5 only operates in the early-acting steps of the mitochondrial ISC assembly machinery donating its $[2Fe\text{-}2S]^{2+}$ cluster to the ISCA1-ISCA2 complex, while the $[2Fe\text{-}2S]^{2+}$ GLRX5-BOLA3 hetero-complex operates downstream specifically in the assembly of a [4Fe-4S] cluster on NFU1. This pathway might be alternative to the pathway involving the [4Fe-4S] cluster transfer from the ISCA1-ISCA2 complex to NFU1. Considering that the *S. cerevisiae* homologue of NFU1 plays a crucial role for the function of mitochondrial [4Fe-4S] enzymes under oxidative metabolism as opposed to anoxic metabolism [8], the here-characterized pathway might be activated under oxidative cellular conditions only. In conclusion, we establish a role of NFU1 as an 'assembler' of [4Fe-4S] clusters alternative to the ISCA1-ISCA2 complex, possibly being operative for a subset of mitochondrial Fe-S target proteins, which are highly susceptible to be damaged in oxidatively growing cells, that is, enzymes with a labile [4Fe-4S] cluster such as aconitase and lipoyl synthase [35]. Moreover, the model shown in Fig. 12 can help to rationalize the complexity observed in human/*S. cerevisiae* NFU1 and BOLA3 phenotypes [4,7–9]. In particular, it was shown that *S. cerevisiae* BolA3 requires *S. cerevisiae* Nfu1 for its function and that Nfu1 and BolA3 cannot mutually substitute each other's biochemical function, even upon overproduction [9]. Thus, these data suggest that BolA3 and Nfu1 perform individual, nonoverlapping functions during the late stages of the mitochondrial ISC machinery, and the here-characterized pathway shows how this cooperative role can be achieved.

We also reported a structural characterization of NFU1 showing that (a) apo NFU1 is present in a monomer-dimer equilibrium, in which the dimer formation is mediated by the N-domain, (b) the two domains in monomeric apo NFU1, although connected by a flexible linker, are not fully independent, (c) that $[4Fe\text{-}4S]^{2+}$ cluster binding to NFU1 causes the quantitative formation of a dimer, (d) that the two NFU1 subunits of the dimer bridge a $[4Fe\text{-}4S]^{2+}$ cluster that is coordinated by two cysteines of each CXXC motif of two C-domains, and (e) the presence of an equilibrium between a $[4Fe\text{-}4S]^{2+}$ NFU1 dimer where the cluster is coordinated by the Cys residues of two CXXC motifs and a $[4Fe\text{-}4S]^{2+}$ NFU1 dimer where a Cys ligand of the CXXC motif is replaced by a S-donor small molecule ligand, such as GSH or DTT. These results are consistent with *in vivo* data reported on *S. cerevisiae* Nfu1 [8]. Indeed, it has been shown that (a) apo Nfu1 in *S. cerevisiae* cells is present as a mixture of a predominant monomer and a minor dimeric species, whose formation is due by the presence of the N-domain of Nfu1; (b) in mitochondrial lysates the bulk of *S. cerevisiae* Nfu1 is a homo-dimeric species, whose abundance is unaffected with DTT but affected by cluster binding. In conclusion, the structural characterization of dimeric $[4Fe\text{-}4S]^{2+}$ NFU1 showed that the cluster has a coordination site accessible to sulfur-containing ligands. This site might be optimal for being invaded by the S-donor ligand of the metal-receiving partner (i.e., the mitochondrial target protein in the presence or not of other possibly required accessory proteins) in order to promote a rapid and controlled cluster-exchange reaction (Fig. 12), following a mechanism typically observed for proteins involved in metal transfer, that is, metallochaperones [36–39].

The recent structural characterization of a construct of human NFU1 42-residue longer at the N terminus

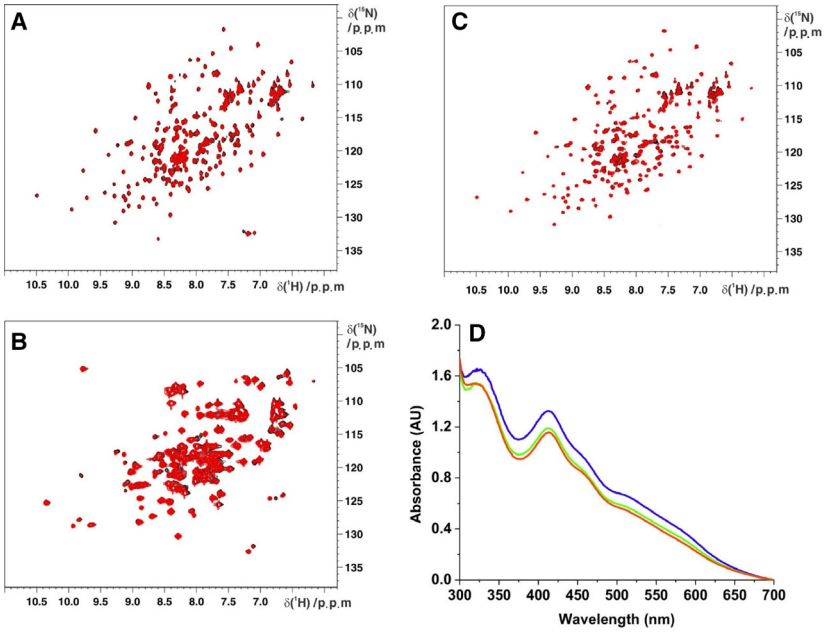

Fig. 11. Both apo and $[2Fe\text{-}2S]^{2+}$ GLRX5 do not interact with mNFU1 and $[2Fe\text{-}2S]^{2+}$ GLRX5 does not assemble a $[4Fe\text{-}4S]^{2+}$ cluster on mNFU1. Overlay of $^{1}H\text{-}^{15}N$ HSQC NMR spectra of: (A) ^{15}N-labeled apo mNFU1 (black) and a 1 : 2 mixture of ^{15}N-labeled apo mNFU1 and unlabeled apo GLRX5 (red); (B) a 60 : 40 mixture of ^{15}N-labeled $[2Fe\text{-}2S]^{2+}$ and apo GLRX5 (black) before and after the addition of two equivalents of apo mNFU1 (red); (C) ^{15}N-labeled apo mNFU1 (black) and a 1 : 2 mixture of ^{15}N-labeled apo mNFU1 and unlabeled $[2Fe\text{-}2S]^{2+}$ GLRX5 (red). NMR spectra were acquired at 298 K in 50 mM phosphate buffer pH 7.0, 5 mM GSH, 5 mM DTT and 150 mM NaCl; (D) UV-visible spectra of $[2Fe\text{-}2S]^{2+}$ GLRX5 (blue), and of a 1 : 2 mixture of mNFU1: $[2Fe\text{-}2S]^{2+}$ GLRX5 (green) and the same mixture after 1 day (red). The UV-vis spectra were acquired at 298 K in 50 mM phosphate buffer pH 7.0, 5 mM GSH, 5 mM DTT, and 150 mM NaCl. UV-vis and NMR experiments were repeated three times.

than mNFU1 sequence showed that the apo protein is monomeric in solution and adopts a dumbbell-shaped structure with well-structured N- and C-domains connected by a flexible linker [16]. It has been also observed that chemically Fe-S cluster reconstituted 42-NFU1 binds a [4Fe-4S] cluster [16]. Combined NMR and SAXS data showed that the holo form of 42-NFU1 is constituted by a trimer of dimers, each containing a [4Fe-4S] cluster [16]. Three N-domains are involved in the formation of a tripartite interface, while two conserved cysteines in the C-domain ligate a [4Fe-4S] cluster to form a dimer by bridging two C-domains. Our NMR data indicate the presence of a single species for $[4Fe\text{-}4S]^{2+}$ NFU1 having a reorientational correlation time of 15.1 ± 1.2 ns, which fully excludes the presence of the trimer of dimers as previously observed for $[4Fe\text{-}4S]^{2+}$ 42-NFU1 [16], while it supports the occurrence of protein dimerization upon cluster binding. Moreover, in the $^{1}H\text{-}^{15}N$ HSQC spectrum of the $[4Fe\text{-}4S]^{2+}$ 42-NFU1, a few residues of the N-domain exhibited two sets of peaks with equal peak volume [16]. They were, respectively, assigned to the free N-domains and to the N-domains that form the tripartite interface in the trimer of dimers of $[4Fe\text{-}4S]^{2+}$ 42-NFU1 [16]. This behavior differs from what we have observed in the $^{1}H\text{-}^{15}N$ HSQC spectrum of our construct for $[4Fe\text{-}4S]^{2+}$ NFU1, which shows indeed only one set of peaks. The different quaternary structure of [4Fe-4S] mNFU1 with respect to that of $[4Fe\text{-}4S]^{2+}$ 42-NFU1 can be rationalized considering that the two NFU1 constructs used in the two studies are different. Indeed, the mitochondrial isoform of NFU1, used in our studies, consists of 59–254 residues [5], while 42-NFU1, previously studied by NMR and SAXS [16], consists of residues 16–254. It might be that the longer N-terminal tail of $[4Fe\text{-}4S]^{2+}$ 42-NFU1 drives the formation of the trimer of dimers binding three [4Fe-4S] clusters. In the structural model of $[4Fe\text{-}4S]^{2+}$ 42-NFU1, the N-domain is, indeed, involved in the formation of the tripartite interface of the trimer [16].

Materials and methods

Protein production

The pETG20A plasmid containing N-terminal tagged mNFU1 (UniProt: Q9UMS0, residues 59–254 with

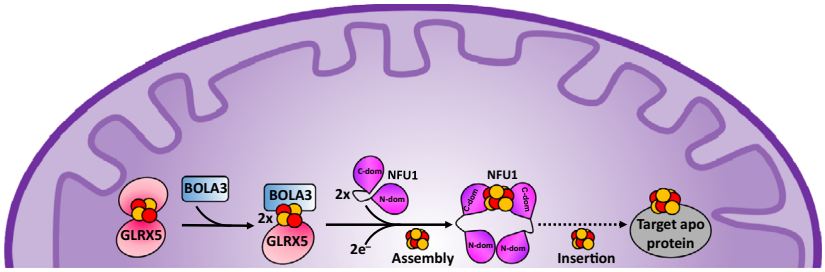

Fig. 12. Model of BOLA3/NFU1-dependent [4Fe-4S] cluster assembly pathway. Two molecules of $[2Fe\text{-}2S]^{2+}$ GLRX5-BOLA3 transfer the cluster to apo NFU1 that assembles a $[4Fe\text{-}4S]^{2+}$ cluster by receiving two electrons. The assembled $[4Fe\text{-}4S]^{2+}$ cluster is then inserted to mitochondrial target apo proteins with or without the requirement of other accessory proteins (dotted arrow).

N-terminal TRX-6His-tag) was used to transform in *E. coli* BL21-Gold(DE3) (Agilent, Santa Clara, CA, USA) competent cells. Cells were cultivated at 37 °C in 1 L of Luria–Bertani (LB) media adding ampicillin (100 $\mu g \cdot mL^{-1}$), until the OD_{600} reached 3–5. The cells were spun down (1693 ***g*** for 20 min) and resuspended in 1 L of fresh LB or minimal media [with 1 g $(^{15}NH_4)_2SO_4$ and 3 g glucose] containing ampicillin (100 $\mu g \cdot mL^{-1}$). The culture was left at 37 °C, 160 r.p.m. for approximately 1 h, and then, protein expression was induced by adding 1 mM of isopropyl β-D-1-thio-galactopyranoside (IPTG), shaking overnight at 30 °C, 160 r.p.m. The cell paste was dissolved in the binding buffer (20 mM phosphate buffer, 500 mM NaCl, 30 mM imidazole, pH 7.8), and the cells were lysated using the CelLytic Express (C1990; Sigma-Aldrich, St. Louis, MO, USA). All the following purification steps were performed aerobically. The N-terminal TRX-6His-tag mNFU1 protein was purified from *E. coli* using a HisTrap HP column (GE Healthcare, Chicago, IL, USA). The TRX-6His-tag was cleaved by tobacco etch virus protease overnight at room temperature in 20 mM phosphate buffer, 500 mM NaCl, 500 mM imidazole, pH 7.8 (UniProt: Q9UMS0, residues 59–254 with N-terminal GSFT residues). The buffer was exchanged to binding buffer, and a second His-trap chromatography column was performed to separate the digested mNFU1 from TRX-6His-tag mNFU1 and TRX-6His-tag. Recovered mNFU1 was pure enough to be used for spectroscopic and biochemical studies. The final yield of apo mNFU1 was ~ 60 mg per liter of LB culture. 2.5 mM tris (2-carboxyethyl) phosphine (TCEP) was added in all the purification steps to avoid disulfide bond formation.

The pETG20A plasmid containing N-domain of mNFU1 (UniProt: Q9UMS0, residues 59–155 with N-terminal TRX-6His-tag; after tag cleavage the N-domain sequence contains N-terminal GSFT residues similarly to the full-length protein) was obtained by a site-directed mutagenesis with a prokaryotic codon stop. The protein expression was performed likewise mNFU1, in BL21-GOLD(DE3) cells. Cells were cultivated at 37 °C in 1 L of LB or minimal media adding ampicillin (100 $\mu g \cdot mL^{-1}$), until the OD_{600} reached 0.6–0.8, and then, protein expression was induced by adding 1 mM of IPTG, shaking overnight at 20 °C, 160 r.p.m. Protein purification steps were performed following the protocol of mNFU1, except that, during TEV protease cleavage, a dialysis step in the binding buffer (20 mM phosphate buffer, 500 mM NaCl, 30 mM imidazole, pH 7.8) was performed. The C-domain of mNFU1 (UniProt: Q9UMS0, residues 162–247 with N-terminal GIDPFTM residues) was cloned by a TOPO cloning reaction (Invitrogen, Carlsbad, CA, USA). The gene was inserted in the pET151/D-TOPO (Invitrogen) vector that present a polyhistidine (6x His) region, a TEV recognition site and a TOPO cloning site. Protein expression and purification steps do not differ from the previously described for the N-domain, and the apo form of C-domain was purified. The final yields of N- and C-domain of mNFU1 were ~ 60 $mg \cdot L^{-1}$ of LB culture. 2.5 mM TCEP was added in all the purification steps to avoid disulfide bond formation.

$[4Fe\text{-}4S]^{2+}$ mNFU1 and $[4Fe\text{-}4S]^{2+}$ C-domain were chemically Fe-S cluster reconstituted in anaerobic conditions in 50 mM Tris(hydroxymethyl)aminomethane hydrochloride, 100 mM NaCl, 5 mM DTT buffer at pH 8.0 with eightfold $FeCl_3$ and Na_2S for 16 h at room temperature. Chemical Fe-S cluster reconstitution was performed with protein concentrations of ~ 40–80 μM. Anaerobic conditions were obtained by degassing all buffers and performing the chemical reconstitution in glove-box with less than 5 p.p.m. of oxygen.

The expression and purification of human BOLA3 and GLRX5 in their apo monomeric forms and in their homo-dimeric (for GLRX5) and hetero-dimeric (for GLRX5-BOLA3) $[2Fe\text{-}2S]^{2+}$ cluster-bound forms were obtained as previously reported [9,10,40].

NMR spectroscopy

1D ^1H paramagnetic-tailored NMR experiments were performed at 400 MHz with a ^1H optimized 5 mm probe at temperatures ranging from 280 and 307 K. Water signal was suppressed via fast repetition experiments and water selective irradiation. Experiments were typically performed using an acquisition time of 50 ms and an overall recycle delay of 90 ms. The protein concentration was 0.5–1 mM, and the spectra were acquired in different buffer conditions

as detailed in the Results section. Squared cosine and exponential multiplications were applied prior to Fourier transformation. Manual baseline correction was performed, using polynomial functions.

^{15}N heteronuclear relaxation experiments on ^{15}N-labeled samples of apo and $[4Fe\text{-}4S]^{2+}$ mNFU1 were recorded on Bruker AVANCE 500 MHz spectrometer at 298 K to measure ^{15}N backbone R_1 and R_2, as well as the heteronuclear ^{15}N[^{1}H] NOEs. Spectra were processed using TopSpin (Bruker BioSpin, Billerica, MA, USA) and analyzed with CARA software (CARA is a free software that can be downloaded fromcara.nmr.ch). The rotational correlation time value was estimated from the R_2/R_1 ratio using the program QUADRATIC_DIFFUSION. The relaxation data for those NHs having an exchange contribution to the R_2 value or exhibiting large-amplitude fast internal motions were excluded from the analysis [41]. NMR relaxation experiments were acquired at 298 K in 50 mM phosphate buffer pH 7.0, 5 mM DTT, and 150 mM NaCl.

SEC-MALS, UV-visible, CD, and NMR spectroscopy for protein–protein interaction studies

SEC-MALS data were aerobically acquired on the apo proteins by attaching a SuperdexTM 200 Increase 10/300 GL column to a DAWN HELEOS system with a continuous flow rate of 0.6 mL·min^{-1} using a filtered degassed buffer (50 mM phosphate buffer, 150 mM NaCl, 5 mM DTT, pH 7.0).

The ^{1}H-^{15}N HSQC NMR spectrum of apo mNFU1 was compared, using CARA software [42], with those of the N- and apo C-domains or with that of $[4Fe\text{-}4S]^{2+}$ mNFU1. The observed chemical shift changes were plotted calculating the backbone weighted average chemical shift differences (Δ_{avg}(HN) (i.e., $(((\Delta H)^2 + (\Delta N/5)^2)/2)^{1/2}$, where ΔH and ΔN are chemical shift differences for backbone amide ^{1}H and ^{15}N nuclei, respectively). Backbone chemical shift assignments of full-length NFU1 and of N- and C-domains of NFU1 in their apo forms were already available in the literature [16]. The ^{1}H-^{15}N HSQC NMR spectra were acquired at 298 K in 50 mM phosphate buffer pH 7.0, 5 mM DTT and 150 mM NaCl.

Protein–protein (or protein–GSH or protein-DTT) interaction, cluster transfer, and assembly experiments were followed performing UV-visible and CD spectra and 2D diamagnetic-tailored ^{1}H-^{15}N HSQC and 1D paramagnetic-tailored ^{1}H NMR experiments in anaerobic conditions. Anaerobic conditions were obtained by degassing all buffers and performing the experiments in glove-box with less than 5 p.p.m. of oxygen. The samples were then sealed in a gas-tight NMR tube or a UV-vis cuvette for the spectroscopic analysis. Each experiment was successfully repeated three times. UV-visible and CD spectra were acquired anaerobically at 298 K in 50 mM phosphate buffer, 5 mM DTT, 150 mM NaCl, pH 7.0 on a Cary 50 Eclipse spectrophotometer (Varian-Agilent Technologies, Palo Alto, CA, USA) and JASCO J-810 spectropolarimeter (JASCO, Easton, MD, USA), respectively. NMR experiments were performed on Bruker AVANCE 400, 700, 900, and 950 MHz spectrometers at 298 K on 0.3–1 mM protein samples. Backbone chemical shift assignments of BOLA3, of BOLA3 in the apo and $[2Fe\text{-}2S]^{2+}$ hetero-complex with GLRX5, of apo GLRX5, and of $[2Fe\text{-}2S]^{2+}$ GLRX5 were already available [10,40]. Chemical shift assignment of the individual N- and C-domains of NFU1 and full-length NFU1 are available in the Biological Magnetic Resonance Bank (under accession codes BMRB: 18489 [NFU1 N-domain], BMRB: 19068 [NFU1 C-domain], and BMRB: 26801 [full-length NFU1]) [16].

The potential interaction between apo mNFU1 and BOLA3 was followed, in 50 mM phosphate buffer, 150 mM NaCl, 5 mM DTT pH 7.0, titrating ^{15}N-labeled (or unlabeled) apo mNFU1 with unlabeled (or ^{15}N-labeled) BOLA3. The potential interaction between $[4Fe\text{-}4S]^{2+}$ mNFU1 and BOLA3 was investigated in anaerobic conditions by (a) chemically reconstituting, in the presence of iron and sulfide ions, equimolar or 1 : 2 mixtures of unlabeled (or ^{15}N-labeled) apo mNFU1 and ^{15}N-labeled (or unlabeled) BOLA3 in 5 mM GSH, 5 mM DTT, 150 mM NaCl, 50 mM Tris base pH 8, or in 5 mM DTT, 150 mM NaCl, 50 mM Tris base pH 8, and spectroscopically investigating the final mixture after having exchanged it in 50 mM phosphate buffer, 150 mM NaCl, 5 mM DTT pH 7.0; (b) titrating a 1 : 1 mixture of ^{15}N-labeled BOLA3 and unlabeled apo GLRX5 with 1 equivalent of $[4Fe\text{-}4S]^{2+}$ mNFU1 in 50 mM phosphate buffer, 150 mM NaCl, 5 mM DTT pH 7.0.

The cluster transfer and assembly observed upon mixing $[2Fe\text{-}2S]^{2+}$ GLRX5-BOLA3 and apo mNFU1 in 50 mM phosphate buffer, 150 mM NaCl, 5 mM GSH, 5 mM DTT pH 7.0 was followed in anaerobic conditions titrating ^{15}N-labeled (or unlabeled) mNFU1 with $[2Fe\text{-}2S]^{2+}$ GLRX5-BOLA3 (unlabeled or ^{15}N-labeled GLRX5 or ^{15}N-labeled BOLA3). The same experiment was also performed in 50 mM phosphate buffer pH 7.0, 5 mM GSH, and 150 mM NaCl.

The potential interaction, cluster transfer, and assembly between GLRX5 and mNFU1 were followed in anaerobic conditions in 50 mM phosphate buffer pH 7.0, 5 mM GSH, 5 mM DTT, and 150 mM NaCl by (a) titrating ^{15}N-labeled apo mNFU1 with unlabeled apo GLRX5; (b) titrating a 60 : 40 mixture of ^{15}N-labeled (or unlabeled) $[2Fe\text{-}2S]^{2+}$ and apo GLRX5 with unlabeled (or ^{15}N-labeled) apo mNFU1.

Molecular docking

The structural model of monomeric apo mNFU1 was calculated using the protein–protein docking program HADDOCK2.2 by following the standard HADDOCK procedure [18,19]. The structures of the individual N- and C-domains (PDB entries 2LTM and 2M5O, respectively)

[16], to which the N- and C-flexible termini have been removed, have been used as input data. The meaningful NMR chemical shift differences, shown in Fig. 2A,B, were used to define ambiguous interaction restraints for the residues at the protein–protein interface. The 'active' residues were defined as those having a chemical shift perturbation upon complex formation larger than the average of Δ_{avg}(HN) plus 1σ and with a solvent accessibility higher than 45%; the 'passive' residues were defined as those being surface neighbors to the active residues and with a solvent accessibility higher than 45%. Following the standard HADDOCK algorithm, HADDOCK clustered 152 structures in eight clusters, which represents 76.0% of the water-refined models HADDOCK generated. The clusters were ranked based on the averaged HADDOCK score of their top four members. The best-scoring HADDOCK cluster resulted in 41 structures, whose statistics are reported in Table 1.

Acknowledgements

The authors acknowledge the support and the use of resources of Instruct-ERIC, a Landmark ESFRI project, and specifically the CERM/CIRMMP Italy Centre. This article is based upon work from COST Action CA15133, supported by COST (European Cooperation in Science and Technology).

Conflict of interest

The authors declare no conflict of interest.

Author contributions

LB and SC-B designed the research; VN, SG, and DS performed research; VN, DS, SC-B, and LB analyzed data; and LB and SC-B wrote the paper.

References

1 Braymer JJ & Lill R (2017) Iron-sulfur cluster biogenesis and trafficking in mitochondria. *J Biol Chem* **292**, 12754–12763.
2 Ciofi-Baffoni S, Nasta V & Banci L (2018) Protein networks in the maturation of human iron-sulfur proteins. *Metallomics* **10**, 49–72.
3 Andreini C, Banci L & Rosato A (2016) Exploiting bacterial operons to illuminate human iron-sulfur proteins. *J Proteome Res*. **15**, 1308–1322.
4 Cameron JM, Janer A, Levandovskiy V, MacKay N, Rouault TA, Tong WH, Ogilvie I, Shoubridge EA & Robinson BH (2011) Mutations in iron-sulfur cluster scaffold genes NFU1 and BOLA3 cause a fatal deficiency of multiple respiratory chain and 2-oxoacid dehydrogenase enzymes. *Am J Hum Genet* **89**, 486–495.
5 Tong WH, Jameson GN, Huynh BH & Rouault TA (2003) Subcellular compartmentalization of human Nfu, an iron-sulfur cluster scaffold protein, and its ability to assemble a [4Fe-4S] cluster. *Proc Natl Acad Sci USA* **100**, 9762–9767.
6 Agar JN, Krebs C, Frazzon J, Huynh BH, Dean DR & Johnson MK (2000) IscU as a scaffold for iron-sulfur cluster biosynthesis: sequential assembly of [2Fe-2S] and [4Fe-4S] clusters in IscU. *Biochemistry* **39**, 7856–7862.
7 Navarro-Sastre A, Tort F, Stehling O, Uzarska MA, Arranz JA, Del TM, Labayru MT, Landa J, Font A, Garcia-Villoria J *et al*. (2011) A fatal mitochondrial disease is associated with defective NFU1 function in the maturation of a subset of mitochondrial Fe-S proteins. *Am J Hum Genet* **89**, 656–667.
8 Melber A, Na U, Vashisht A, Weiler BD, Lill R, Wohlschlegel JA & Winge DR (2016) Role of Nfu1 and Bol3 in iron-sulfur cluster transfer to mitochondrial clients. *Elife*. **5**, e15991.
9 Uzarska MA, Nasta V, Weiler BD, Spantgar F, Ciofi-Baffoni S, Saviello M, Gonnelli L, Muhlenhoff U, Banci L & Lill R (2016) Mitochondrial Bol1 and Bol3 function as assembly factors for specific iron-sulfur proteins. *Elife* **5**, e16673.
10 Nasta V, Giachetti A, Ciofi-Baffoni S & Banci L (2017) Structural insights into the molecular function of human (2Fe-2S) BOLA1-GRX5 and (2Fe-2S) BOLA3-GRX5 complexes. *Biochim Biophys Acta* **1861**, 2119–2131.
11 Uzarska MA, Dutkiewicz R, Freibert SA, Lill R & Muhlenhoff U (2013) The mitochondrial Hsp70 chaperone Ssq1 facilitates Fe/S cluster transfer from Isu1 to Grx5 by complex formation. *Mol Biol Cell* **24**, 1830–1841.
12 Nakai K & Horton P (1999) PSORT: a program for detecting sorting signals in proteins and predicting their subcellular localization. *Trends Biochem Sci* **24**, 34–36.
13 Emanuelsson O (2002) Predicting protein subcellular localisation from amino acid sequence information. *Brief Bioinform* **3**, 361–376.
14 Liu Y & Cowan JA (2007) Iron sulfur cluster biosynthesis. Human NFU mediates sulfide delivery to ISU in the final step of [2Fe-2S] cluster assembly. *Chem Commun (Cambridge)* **30**, 3192–3194.
15 Lebigot E, Gaignard P, Dorboz I, Slama A, Rio M, de Lonlay P, Heron B, Sabourdy F, Boespflug-Tanguy O, Cardoso A *et al*. (2017) Impact of mutations within the [Fe-S] cluster or the lipoic acid biosynthesis pathways on mitochondrial protein expression profiles in fibroblasts from patients. *Mol Genet Metab* **122**, 85–94.
16 Cai K, Liu G, Frederick RO, Xiao R, Montelione GT & Markley JL (2016) Structural/functional properties of human NFU1, an intermediate [4Fe-4S] carrier in

human mitochondrial iron-sulfur cluster biogenesis. *Structure* **24**, 2080–2091.
17 Shapiro YE, Sinev MA, Sineva EV, Tugarinov V & Meirovitch E (2000) Backbone dynamics of *Escherichia coli* adenylate kinase at the extreme stages of the catalytic cycle studied by (15)N NMR relaxation. *Biochemistry* **39**, 6634–6644.
18 Dominguez C, Boelens R & Bonvin AM (2003) HADDOCK: a protein-protein docking approach based on biochemical or biophysical information. *J Am Chem Soc* **125**, 1731–1737.
19 van Zundert GC, Rodrigues JP, Trellet M, Schmitz C, Kastritis PL, Karaca E, Melquiond AS, van Dijk M, de Vries SJ & Bonvin AM (2016) The HADDOCK2.2 web server: user-friendly integrative modeling of biomolecular complexes. *J Mol Biol* **428**, 720–725.
20 Freibert SA, Weiler BD, Bill E, Pierik AJ, Muhlenhoff U & Lill R (2018) Biochemical reconstitution and spectroscopic analysis of iron-sulfur proteins. *Methods Enzymol* **599**, 197–226.
21 Bandyopadhyay S, Naik SG, O'Carroll IP, Huynh BH, Dean DR, Johnson MK & Dos Santos PC (2008) A proposed role for the *Azotobacter vinelandii* NfuA protein as an intermediate iron-sulfur cluster carrier. *J Biol Chem* **283**, 14092–14099.
22 Banci L, Camponeschi F, Ciofi-Baffoni S & Piccioli M (2018) The NMR contribution to protein-protein networking in Fe-S protein maturation. *J Biol Inorg Chem* **23**, 665–685.
23 Mapolelo DT, Zhang B, Naik SG, Huynh BH & Johnson MK (2012) Spectroscopic and functional characterization of iron-sulfur cluster-bound forms of *Azotobacter vinelandii* (Nif)IscA. *Biochemistry* **51**, 8071–8084.
24 Chandramouli K, Unciuleac MC, Naik S, Dean DR, Huynh BH & Johnson MK (2007) Formation and properties of [4Fe-4S] clusters on the IscU scaffold protein. *Biochemistry* **46**, 6804–6811.
25 Brancaccio D, Gallo A, Mikolajczyk M, Zovo K, Palumaa P, Novellino E, Piccioli M, Ciofi-Baffoni S & Banci L (2014) Formation of [4Fe-4S] clusters in the mitochondrial iron-sulfur cluster assembly machinery. *J Am Chem Soc* **136**, 16240–16250.
26 Ewen KM, Ringle M & Bernhardt R (2012) Adrenodoxin–a versatile ferredoxin. *IUBMB Life* **64**, 506–512.
27 Sheftel AD, Stehling O, Pierik AJ, Elsasser HP, Muhlenhoff U, Webert H, Hobler A, Hannemann F, Bernhardt R & Lill R (2010) Humans possess two mitochondrial ferredoxins, Fdx1 and Fdx2, with distinct roles in steroidogenesis, heme, and Fe/S cluster biosynthesis. *Proc Natl Acad Sci USA* **107**, 11775–11780.
28 Shi Y, Ghosh M, Kovtunovych G, Crooks DR & Rouault TA (2012) Both human ferredoxins 1 and 2 and ferredoxin reductase are important for iron-sulfur cluster biogenesis. *Biochim Biophys Acta* **1823**, 484–492.
29 Sheftel AD, Wilbrecht C, Stehling O, Niggemeyer B, Elsasser HP, Muhlenhoff U & Lill R (2012) The human mitochondrial ISCA1, ISCA2, and IBA57 proteins are required for [4Fe-4S] protein maturation. *Mol Biol Cell* **23**, 1157–1166.
30 Beilschmidt LK, Ollagnier de Choudens S, Fournier M, Sanakis I, Hograindleur MA, Clemancey M, Blondin G, Schmucker S, Eisenmann A, Weiss A *et al.* (2017) ISCA1 is essential for mitochondrial Fe4S4 biogenesis *in vivo*. *Nat Commun* **8**, 15124.
31 Brancaccio D, Gallo A, Piccioli M, Novellino E, Ciofi-Baffoni S & Banci L (2017) [4Fe-4S] cluster assembly in mitochondria and its impairment by copper. *J Am Chem Soc* **139**, 719–730.
32 Gourdoupis S, Nasta V, Calderone V, Ciofi-Baffoni S & Banci L (2018) IBA57 recruits ISCA2 to form a [2Fe-2S] cluster-mediated complex. *J Am Chem Soc* **140**, 14401–14412.
33 Floyd BJ, Wilkerson EM, Veling MT, Minogue CE, Xia C, Beebe ET, Wrobel RL, Cho H, Kremer LS, Alston CL *et al.* (2016) Mitochondrial protein interaction mapping identifies regulators of respiratory chain function. *Mol Cell* **63**, 621–632.
34 Sen S, Rao B, Wachnowsky C & Cowan JA (2018) Cluster exchange reactivity of [2Fe-2S] cluster-bridged complexes of BOLA3 with monothiol glutaredoxins. *Metallomics* **10**, 1282–1290.
35 McCarthy EL & Booker SJ (2017) Destruction and reformation of an iron-sulfur cluster during catalysis by lipoyl synthase. *Science* **358**, 373–377.
36 Robinson NJ & Winge DR (2010) Copper metallochaperones. *Annu Rev Biochem* **79**, 537–562.
37 Banci L, Bertini I, Cantini F & Ciofi-Baffoni S (2010) Cellular copper distribution: a mechanistic systems biology approach. *Cell Mol Life Sci* **67**, 2563–2589.
38 O'Halloran TV & Culotta VC (2000) Metallochaperones: an intracellular shuttle service for metal ions. *J Biol Chem* **275**, 25057–25060.
39 Boal AK & Rosenzweig AC (2009) Structural biology of copper trafficking. *Chem Rev* **109**, 4760–4779.
40 Banci L, Brancaccio D, Ciofi-Baffoni S, Del Conte R, Gadepalli R, Mikolajczyk M, Neri S, Piccioli M & Winkelmann J (2014) [2Fe-2S] cluster transfer in iron-sulfur protein biogenesis. *Proc Natl Acad Sci USA* **111**, 6203–6208.
41 Banci L, Bertini I, Cantini F, Ciofi-Baffoni S, Cavet JS, Dennison C, Graham AI, Harvie DR & Robinson NJ (2007) NMR structural analysis of cadmium-sensing by winged helix repressor CMTR. *J Biol Chem* **282**, 30181–30188.
42 Keller R (2004) The Computer Aided Resonance Assignment Tutorial. CANTINA Verlag, Goldau.